European Journal of Mechanics B/Fluids 33 (2012) 95–104

Contents lists available at SciVerse ScienceDirect

European Journal of Mechanics B/Fluids

journal homepage: www.elsevier.com/locate/ejmflu

Buoyancy-driven heat transfer analysis in two-square duct annuli filled with a nanofluid

A. Arefmanesh [a], M. Amini [a,*], M. Mahmoodi [a], M. Najafi [b]

[a] Department of Mechanical Engineering, University of Kashan, Kashan, Iran

[b] Mechanical and Aerospace Engineering Department, Islamic Azad University, Science and Research Branch, Tehran, Iran

ARTICLE INFO

Article history:
Received 17 April 2011
Received in revised form
26 September 2011
Accepted 23 November 2011
Available online 3 December 2011

Keywords:
Natural convection
Nanofluid
Annulus
Finite volume method
Square duct

ABSTRACT

The natural convection fluid flow and heat transfer in the annuli of two differentially-heated square ducts filled with the TiO_2-water nanofluid are investigated numerically. The outer duct is maintained at a constant temperature T_c while the inner duct is kept at a differentially higher constant temperature T_h. The governing equations written in terms of the primitive variables are solved using the finite volume method and the SIMPLER algorithm. Through a parametric study conducted, the effects of the Rayleigh number, the aspect ratio of the annulus, and the volume fraction of the nanoparticles on the fluid flow and heat transfer are investigated. To verify the numerical procedure, two different natural convection simulations are conducted using the proposed code, and the results are found to be in good agreement with the existing results already available in the literature. The numerical outcome of the present study shows that, by increasing the width of the gap between the ducts and also the Rayleigh number, multiple eddies are developed in the gap between the top walls of the square ducts. The eddies formed demonstrate the characteristics of the Rayleigh–Bénard convective type. Moreover, it is observed from the results that, the average Nusselt number increases by increasing the volume fraction of the nanoparticles.

1. Introduction

Buoyancy-driven fluid flow and heat transfer in the annuli are encountered in a number of industrial applications such as heat exchangers, home ventilation, and electronic cooling devices. Low thermal conductivity of conventional fluids such as water and oil is a heat transfer drawback in heat exchangers. Heat transfer in such devices can be enhanced by using nanofluid media, for their higher thermal conductivity. A comprehensive review of the nanofluid heat transfer characteristics can be found in Godson et al. [1].

As far as natural convection transfer of heat utilizing nanofluids, Buongiorno [2] conducted a property study of nanofluids to develop an explanation for the abnormal conductive heat transfer enhancement observed in them. Among his major findings, an order-of-magnitude estimation for various terms of the energy equation suggested that energy transfer by nanoparticle dispersion is negligible contrary to what is commonly stated in the literature. He also found that convective heat transfer enhancement can be explained mainly with a reduction of viscosity within and consequent thinning of the laminar sublayer. Khanafer et al. [3] investigated the buoyancy-driven fluid flow and heat transfer in rectangular cavities filled with nanofluids numerically. They concluded that, for the considered range of the Grashof numbers, the Nusselt number increased with increasing the volume fraction of the nanoparticles. Jou and Tzeng [4] studied the natural convection fluid flow and heat transfer in rectangular cavities filled with Cu–water nanofluid using the finite difference method. They showed that the heat transfer coefficient increased by increasing the Rayleigh number and the volume fraction of the nanoparticles. In another study, Abu-Nada et al. [5] conducted numerical analyses of the buoyancy-driven heat transfer in the horizontal annuli of differentially-heated concentric cylinders filled with nanofluids using the finite volume method. They examined different water based nanofluids containing Cu, Ag, Al_2O_3, and TiO_2 solid particles. Based on their observations, for high Rayleigh numbers, the heat transfer was significantly enhanced for the nanoparticles with high thermal conductivity, while for intermediate values of the Rayleigh number, nanoparticles with low thermal conductivity showed some reductions of heat transfer. Santra et al. [6] studied the free convection of Cu–water nanofluid in a differentially-heated square cavity. They observed that the heat transfer decreased with increasing the volume fraction of the nanoparticles for Rayleigh numbers between 10^4 and 10^7. Moreover, their results showed that, the heat transfer increased with increasing the Rayleigh number for some particular nanoparticles volume fractions they had considered. Oztop and Abu-nada [7], using the finite volume method, carried out a numerical study on the free convection heat

* Corresponding author. Tel.: +98 913 2722848.
E-mail address: meysamini@yahoo.com (M. Amini).

0997-7546/$ – see front matter © 2011 Elsevier Masson SAS. All rights reserved.
doi:10.1016/j.euromechflu.2011.11.004

Nomenclature

AR	Aspect ratio
c_p	Heat capacity
g	Gravitational acceleration, m/s^2
h	Height of inner square, m
H	Height of outer square, m
k	Thermal conductivity, W/m–K
Nu	Nusselt number
p	Pressure, kg/m s^2
P	Dimensionless pressure
Pr	Prandtl number
Ra	Rayleigh number
T	Temperature, K
u, v	Velocity components, m/s
U, V	Dimensionless velocity components
x, y	Cartesian coordinates, m
X, Y	Dimensionless Cartesian coordinates

Greek letters

α	Thermal diffusivity, m^2/s
β	Thermal expansion coefficient, 1/K
μ	Viscosity, kg/m-s
υ	Kinematics viscosity, m^2/s
θ	Dimensionless temperature
ρ	Density, kg/m^3
φ	Volume fraction of nanoparticles

Subscript

avg	Average
c	Cold
f	Fluid
h	Hot
nf	Nanofluid
p	Particle

transfer in rectangular cavities. Their considered cavity comprises a cold vertical wall, an embedded heater counterpart wall, and insulated horizontal walls. They considered the effects of the Rayleigh number, the cavity aspect ratio, the size and the location of the heater on the wall, and the type of nanofluid on the heat transfer within the cavity. Their results showed an increase in the average Nusselt number with increasing the volume fraction of the nanoparticles for Rayleigh numbers between 10^3 and 10^5.

More recently, Abu-nada and Oztop [8] used the finite volume method to study the buoyancy-driven fluid flow and heat transfer in an inclined square cavity filled with Cu–water nanofluid. They showed that the inclination angle of the enclosure played an important role on the cavity fluid flow and heat transfer. Their results indicated that the addition of copper nanoparticles to the base fluid resulted in a remarkable heat transfer enhancement. Furthermore, it was observed that the effect of the inclination angle on the heat transfer enhancement became insignificant at low Rayleigh number. Ögüt [9] studied the natural convection in an inclined square cavity with insulated top and bottom walls, a cold right wall, and an embedded heater left wall. In his investigations the cavity was filled with different water-based nanofluids. Using polynomial differential quadrature method, he observed that the average heat transfer rate increased significantly as the nanoparticles volume fraction and the Rayleigh number increased. Moreover, his results indicated that the average heat transfer decreased with increasing the length of the heater. Aminossadati and Ghasemi [10] used the finite volume method to investigate the buoyancy-driven fluid flow and heat transfer in a square cavity having a constant flux heater on its horizontal bottom wall. The rest of the cavity walls were kept at a relatively lower temperature. The cavity was filled with different water-based nanofluids. They investigated the effects of the Rayleigh number, the nanoparticles volume fraction, the size and location of the heater, and the type of the nanoparticles on the heat transfer inside the cavity. Their results indicated that adding nanoparticles to pure water improved the heat transfer performance especially at low Rayleigh numbers. In another study, Ghasemi and Aminossadati [11] investigated periodic buoyancy-driven fluid flow and heat transfer in a square cavity filled with different water-based nanofluids. The cavity had insulated top and bottom walls, a cold right vertical wall, and an oscillating flux heat source on its left vertical wall. Their results showed that adding nanoparticles, in particular Cu, to the base fluid enhanced the heat transfer especially at low Rayleigh numbers. Furthermore, they observed periodic profiles for the flow and temperature fields due to the oscillating heat flux. Moreover, the optimum position of the heat source on the left wall was found to be a function of the Rayleigh number. Gumguma and Tezer-Sezgin [12] used the dual reciprocity boundary element method to investigate the unsteady natural convection flow of nanofluids in square cavities having a heat source. Their results showed that the average Nusselt number increased with increasing the volume fraction of the nanoparticles and the Rayleigh number. It was also observed that an increase in the heater length reduced the heat transfer rate.

Very recently, Ni et al. [13] conducted an experimental investigation of turbulent thermal convection in water-based alumina nanofluid between two plates under the condition of fixed temperature at the top plate and fixed input heat flux at the bottom one. They observed that the convective heat transfer coefficient, Nusselt number, and Rayleigh number decreased with increasing the volume fraction of the nanoparticles. In contrast, the velocity of the convective flow showed no significant change over the range of the considered nanoparticle concentrations. Free convection heat transfer enhancement in a square cavity based on experimental measured conductivity was investigated by Jahanshahi et al. [14]. The numerical simulation was subjected to different side wall temperatures using water–SiO_2 nanofluid for the Rayleigh number of the base fluid, $Ra = 10^5 - 10^7$, and the volumetric fraction of nanoparticle between 0% and 4%. An experimental setup was used to extract the conductivity value of the nanofluid. The study showed that the average Nusselt number increased with the volume fraction for the whole range of Rayleigh numbers used.

Among very recent numerical works, Oztop et al. [15] investigated a steady state natural convection in an inclined square enclosure filled with a nanofluid subjected to heating and cooling by sinusoidal temperature profiles on one side of the cavity using the finite volume method. The study reported an enhancement in heat transfer rate for the whole range of considered Rayleigh numbers. However, low Rayleigh numbers showed more enhancement compared to high Rayleigh numbers. In two different studies of free convection in partially-heated side walls square cavities by Sheikhzadeh et al. [16,17], finite volume method was utilized to solve the two-dimensional governing equations for both square cavities with different boundary conditions filled with TiO_2–water nanofluid in one work and Cu–water nanofluid in the other. Their results for the TiO_2–water nanofluid show that by increasing the volume fraction of the nanoparticles, the average Nusselt number of the hot wall increases for the shallow cavities and a reverse trend takes place for the tall ones. However, for the Cu–water nanofluid the average Nusselt number increases with increasing both the Rayleigh number and the volume fraction of the nanoparticles.

In an analytical–numerical work in 2011, Alloui et al. [18] investigated the natural convection in a shallow rectangular

cavity filled with nanofluids. Neumann boundary conditions for temperature were applied to the horizontal walls of the enclosure, while the two vertical ones were assumed insulated. The stability of the convective motion, predicted by parallel flow approximation, was investigated numerically on the basis of the linear stability theory. Among the main conclusions, the enhancement of heat transfer, due to presence of nanoparticles, was found to depend on both the Rayleigh number and the volume fraction of the nanofluid. In another work, Ghasemi and Aminossadati [19] numerically investigated the natural convection heat transfer in a right triangular enclosure having a heat source on its vertical wall filled with CuO–water nanofluid. They considered the effects of different parameters such as the Rayleigh number, the nanoparticles volume fraction, the heat source location on the wall, and the Brownian motion on the flow and temperature fields. Their results showed that, the heat transfer rate increased continuously with increasing the nanoparticles volume fraction at low Rayleigh numbers. However, an optimum solid volume fraction was determined to exist which would result the maximum heat transfer rate at high Rayleigh numbers.

A detailed review of the exciting literature reveals that, although many studies have been conducted on natural convection heat transfer within the annuli of many coaxial basic geometries containing conventional fluids, no investigations devoting to the fluid flow and natural convection analysis on a nanofluid within many basic annuli geometries such as the annulus of two-square duct have been reported. The present study, therefore, concentrates on the analysis of a nanofluid flow and buoyancy-driven heat transfer within a two-dimensional, differentially heated annulus of two concentric square ducts.

2. Problem formulation

Consider the two concentric ducts depicted schematically in Fig. 1. Each side of the inner square and also each side of the outer square is denoted h and H, respectively. The aspect ratio of the annulus is defined as $AR = h/H$. The length of the inner and the outer ducts perpendicular to the plane of the figure are long enough for the problem to be considered two-dimensional. The inner and outer squares are maintained at a differentially-different constant temperatures of T_h and T_c, respectively, with $T_h > T_c$. The annulus (the space between the two-squares) is filled with a nanofluid composed of water and TiO_2 spherical nanoparticles. The nanofluid is assumed to be incompressible, and the nanoparticles are presumed to be in thermal equilibrium with the water. Moreover, there is no slip between the nanoparticles and the base fluid. The thermophysical properties of the base fluid and the nanoparticles are presented in Table 1. The properties of the nanofluid are assumed to be constant with the exception of its density which varies according to the Boussinesq approximation [20].

The continuity, x- and y- components of momentum, and energy equations for the two-dimensional steady and laminar nanofluid flow are given in Eqs. (1)–(4), respectively. The natural convection term through the Boussinesq approximation is incorporated into the y component of momentum (Eq. (3)).

$$\frac{\partial u}{\partial x}+\frac{\partial v}{\partial y}=0, \tag{1}$$

$$u\frac{\partial u}{\partial x}+v\frac{\partial u}{\partial y}=-\frac{1}{\rho_{nf}}\frac{\partial p}{\partial x}+\frac{\mu_{nf}}{\rho_{nf}}\left(\frac{\partial^2 u}{\partial x^2}+\frac{\partial^2 u}{\partial y^2}\right), \tag{2}$$

$$u\frac{\partial v}{\partial x}+v\frac{\partial v}{\partial y}=-\frac{1}{\rho_{nf}}\frac{\partial p}{\partial y}+\frac{\mu_{nf}}{\rho_{nf}}\left(\frac{\partial^2 v}{\partial x^2}+\frac{\partial^2 v}{\partial y^2}\right)+\frac{(\rho\beta)_{nf}\,g\,(T-T_c)}{\rho_{nf}}, \tag{3}$$

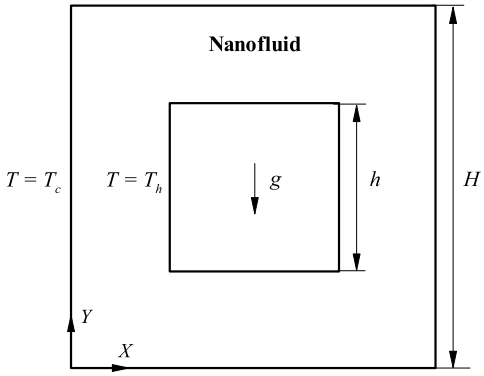

Fig. 1. Schematic of the concentric squares with boundary conditions.

Table 1
Thermophysical properties of the base fluid and nanoparticles [7].

Physical properties	Base fluid (water)	Nanoparticles (TiO_2)
C_p (J/kg-K)	4179	686.2
ρ (kg/m^3)	997.1	4250
k (W/m–K)	0.613	8.9538
$\beta \times 10^5$ (K^{-1})	21	0.9
μ (kg/m-s)	0.001003	–

and

$$u\frac{\partial T}{\partial x}+v\frac{\partial T}{\partial y}=\alpha_{nf}\left(\frac{\partial^2 T}{\partial x^2}+\frac{\partial^2 T}{\partial y^2}\right). \tag{4}$$

In order to cast the governing equations into a dimensionless form, the following dimensionless variables are introduced:

$$X=\frac{x}{H},\quad Y=\frac{y}{H},\quad U=\frac{uH}{\alpha_f},\quad V=\frac{vH}{\alpha_f},\quad P=\frac{pH^2}{\rho_{nf}\,\alpha_f^2},\quad \text{and}\quad \theta=\frac{T-T_c}{T_h-T_c}. \tag{5}$$

Substituting the above dimensionless variables into the continuity, momentum, and energy equations results in the following dimensionless form of the governing equations:

$$\frac{\partial U}{\partial X}+\frac{\partial V}{\partial Y}=0, \tag{6}$$

$$U\frac{\partial U}{\partial X}+V\frac{\partial U}{\partial Y}=-\frac{\partial P}{\partial X}+\frac{\mu_{nf}}{\rho_{nf}\alpha_f}\left(\frac{\partial^2 U}{\partial X^2}+\frac{\partial^2 U}{\partial Y^2}\right), \tag{7}$$

$$U\frac{\partial V}{\partial X}+V\frac{\partial V}{\partial Y}=-\frac{\partial P}{\partial Y}+\frac{\mu_{nf}}{\rho_{nf}\alpha_f}\left(\frac{\partial^2 V}{\partial X^2}+\frac{\partial^2 V}{\partial Y^2}\right)+\frac{(\rho\beta)_{nf}}{\rho_{nf}\,\beta_f}Ra\,Pr\,\theta, \tag{8}$$

and

$$U\frac{\partial \theta}{\partial X}+V\frac{\partial \theta}{\partial Y}=\frac{\alpha_{nf}}{\alpha_f}\left(\frac{\partial^2 \theta}{\partial X^2}+\frac{\partial^2 \theta}{\partial Y^2}\right), \tag{9}$$

where the Rayleigh number Ra, and the Prandtl number Pr are defined as follows:

$$Ra=\frac{g\beta_f\,\Delta T\,H^3}{\alpha_f\nu_f},\quad \text{and}\quad Pr=\frac{\nu_f}{\alpha_f}. \tag{10}$$

The boundary conditions for Eqs. (6)–(9) are

$$\begin{aligned} &U=V=0,\qquad \theta=1\quad \text{on the inner square,}\\ &\text{and}\\ &U=V=0,\qquad \theta=0\quad \text{on the outer square.}\end{aligned} \tag{11}$$

2.1. Thermophysical properties of the nanofluid

The effective viscosity, μ_{nf}, and the thermal conductivity, k_{nf}, of the nanofluid are obtained from the following respective relations proposed by He et al. based on their experimental results [21]

$$\mu_{nf} = \mu_f \left(199.21\varphi^2 + 4.62\varphi + 1.0\right), \tag{12}$$

and

$$k_{nf} = k_f \left(125.62\varphi^2 + 4.82\varphi + 1.0\right). \tag{13}$$

The density, ρ_{nf}, the heat capacity, $(\rho c_p)_{nf}$, and the thermal expansion coefficient, $(\rho\beta)_{nf}$, of the nanofluid are obtained from the following respective equations [7–10]:

$$\rho_{nf} = (1-\varphi)\,\rho_f + \varphi\,\rho_p, \tag{14}$$

$$\left(\rho c_p\right)_{nf} = (1-\varphi)\left(\rho c_p\right)_f + \varphi\,\left(\rho c_p\right)_p, \tag{15}$$

and

$$(\rho\beta)_{nf} = (1-\varphi)\,(\rho\beta)_f + \varphi\,(\rho\beta)_p. \tag{16}$$

The thermal diffusivity of the nanofluid α_{nf} is evaluated from

$$\alpha_{nf} = \frac{k_{nf}}{\left(\rho c_p\right)_{nf}}. \tag{17}$$

The Nusselt number based on the height (or width) of the outer square is evaluated from the following relation:

$$Nu = \frac{h_{nf} H}{k_f}. \tag{18}$$

The heat transfer coefficient for the nanofluid h_{nf} is obtained from

$$h_{nf} = \frac{q}{T_h - T_c}, \tag{19}$$

where the wall heat flux per unit area q can be written as

$$q = -k_{nf}\frac{T_h - T_c}{H}\left.\frac{\partial\theta}{\partial n}\right|_{wall}. \tag{20}$$

Substituting Eqs. (19) and (20) into Eq. (18) yields the following relation for the Nusselt number

$$Nu = -\left(\frac{k_{nf}}{k_f}\right)\left.\frac{\partial\theta}{\partial n}\right|_{wall}. \tag{21}$$

3. Numerical implementation

The mass, momentum, and energy governing equations written in terms of the primitive variables are discretized using the finite volume approach and the SIMPLER algorithm. In this method [22], a regular two-dimensional finite difference mesh is generated in the computational domain. Subsequently, a square-shaped control volume is generated around each nodal point. The governing equations are then integrated over each control volume. Subsequently, the derivatives of the dependent variables on the faces of the control volume in the resulting equations are replaced by finite difference forms written in terms of the nodal values of the dependent variables. A second-order central difference scheme is used for the diffusion terms while a hybrid scheme, a combination of upwind and central difference schemes, is employed for the convective terms [22]. Carrying out the same procedure for all the control volumes yields a system of algebraic equations with nodal values of the dependent variables as unknowns. The set of discretized equations are then solved iteratively yielding the velocity, pressure, and temperature at the nodal points. An under-relaxation scheme is employed to obtain converged solutions.

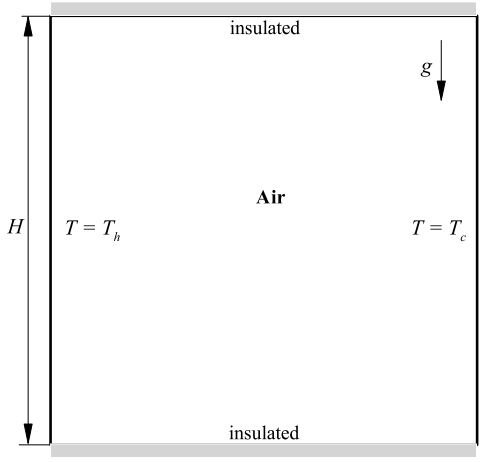

Fig. 2. Domain and boundary conditions for the buoyancy-driven heat transfer in a square cavity filled with air.

3.1. Benchmarking of the code

In order to validate the numerical procedure, two simulations of a buoyancy-driven fluid flow and heat transfer in a differentially-heated square cavity filled with air, and a natural convection heat transfer in a partially-heated square cavity filled with the Cu–water nanofluid are performed using the proposed code, and the results are compared with the existing results in the literature.

The domain and the boundary conditions for the natural convection heat transfer in a differentially-heated square cavity are shown in Fig. 2. The left and the right side walls of the cavity are maintained at constant temperatures T_h and T_c, respectively, with $T_h > T_c$. The cavity's top and bottom walls are insulated. The cavity is filled with air ($Pr = 0.72$), and the simulations are performed for a range of Rayleigh numbers from 10^3 to 10^6. Table 2 shows comparisons between the average Nusselt numbers of the hot wall obtained by the present simulation with the results of other investigations [3,23–26] for different Rayleigh numbers. As the table shows, very good agreements exist between the results of the current simulation and those of other investigators for the considered range of Rayleigh numbers.

The domain and the boundary conditions for the buoyancy-driven heat transfer in a partially-heated square cavity filled with Cu–water nanofluid are shown in Fig. 3. A heat source of constant temperature T_h, whose length is equal to half of the cavity's height, is placed symmetrically along the left wall of the cavity. The right side wall of the cavity is maintained at a constant temperature T_c with $T_c < T_h$. The top and bottom walls as well as the remaining portion of the left side wall are kept insulated. The simulations are performed for different volume fractions of the nanoparticles including $\varphi = 0$ (pure water), for $Ra = 10^3$, 10^4, and 10^5. Table 3 shows comparisons between the average Nusselt number of the heat source obtained by the present simulation with the results of Oztop and Abu-Nada [7] for different volume fractions of the nanoparticles at different Rayleigh numbers. As it is observed from the table, very good agreements exist between the two results for the considered ranges of the Rayleigh numbers and volume fractions of the nanoparticles.

3.2. Grid independence study

In order to determine a proper grid for the numerical simulations, a grid independence study is conducted for the natural convection heat transfer in the space between concentric squares shown in Fig. 1. The considered aspect ratio is $AR = 1/2$, and the calculations are performed for TiO_2–water nanofluid with

Table 2
Average Nusselt number for differentially-heated square cavity filled with air, comparisons with the results of other investigators.

	$Ra = 10^3$	$Ra = 10^4$	$Ra = 10^5$	$Ra = 10^6$
Present study	1.113	2.254	4.507	8.802
Barakos and Mitsoulis [23]	1.114	2.245	4.510	8.806
Davis [24]	1.118	2.243	4.519	8.799
Faseqi et al. [25]	1.105	2.302	4.646	9.012
Khanafer et al. [3]	1.118	2.245	4.522	8.826
Markatos and Pericleous [26]	1.108	2.201	4.430	8.754

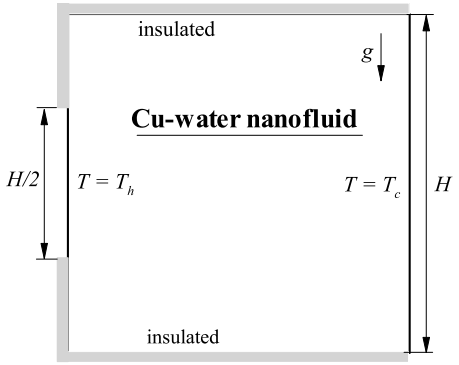

Fig. 3. Domain and boundary conditions for the buoyancy-driven heat transfer in a square cavity with a partially-heated wall filled with Cu–water nanofluid.

Table 3
Average Nusselt number of the heat source, comparison with Oztop and Abu-Nada [7] for the partially-heated square cavity filled with Cu–water nanofluid.

Ra	φ	Present study	Oztop and Abu–Nada [7]
10^3	0.00	1.045	1.004
	0.05	1.131	1.122
	0.10	1.255	1.251
	0.15	1.450	1.423
	0.20	1.665	1.627
10^4	0.00	2.001	2.010
	0.05	2.098	2.122
	0.10	2.155	2.203
	0.15	2.276	2.283
	0.20	2.355	2.363
10^5	0.00	3.973	3.983
	0.05	4.266	4.271
	0.10	4.352	4.440
	0.15	4.651	4.662
	0.20	4.865	4.875

$\varphi = 0.02$ at $Ra = 10^6$. Six different uniform grids, namely, $21 \times 21, 41 \times 41, 61 \times 61, 81 \times 81, 100 \times 100$, and 121×121 are employed for the numerical simulations. Fig. 4 shows the vertical velocity component along the horizontal centreline of the annulus ($Y = H/2$, Fig. 1) for these grids. The results for the average Nusselt number of the inner square for the above uniform grids are also presented in Table 4. It is observed from Fig. 4 and Table 4 that an 81×81 uniform grid is sufficiently fine to capture the temperature and velocity variations in the boundary layers adjacent to the wall. Therefore, based on these results, an 81×81 uniform grid is employed to perform all of the subsequent numerical calculations. Moreover, in these numerical simulations, the convergence criterion for temperature, pressure, and velocity is

$$Error = \frac{\sum_{j=1}^{m}\sum_{i=1}^{n}\left|\xi_{i,j}^{t+1} - \xi_{i,j}^{t}\right|}{\sum_{j=1}^{m}\sum_{i=1}^{n}\left|\xi_{i,j}^{t+1}\right|} \leq 10^{-7}, \tag{22}$$

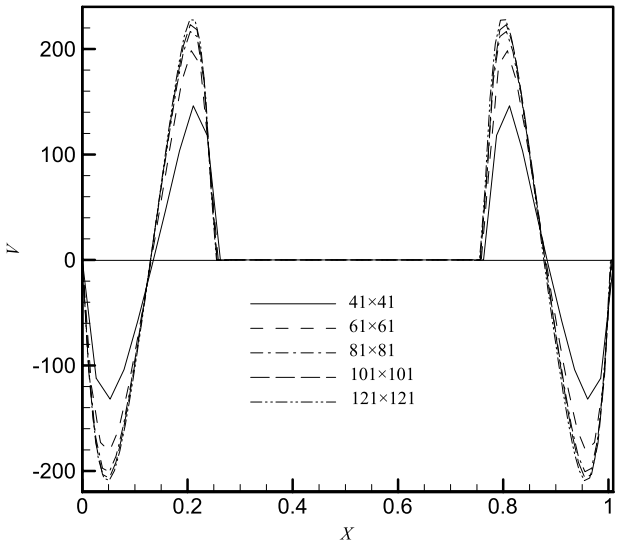

Fig. 4. Vertical velocity component along the horizontal centreline of the annulus ($Y = H/2$, Fig. 1) for different uniform grids, $AR = 1/2$, $\varphi = 0.02$, and $Ra = 10^6$.

where m and n are the number of grid points in x- and y-directions, respectively, ξ is any of the computed field variables, and t is the iteration number.

4. Results and discussions

Having verified the numerical procedure via performing two simulations, the proposed code is employed to study the buoyancy-driven fluid flow and heat transfer in the space between two concentric squares, (Fig. 1), filled with TiO_2–water nanofluid. The results discussed here are for three aspect ratios of 1/4, 1/2, and 3/4, a range of Rayleigh numbers from 10^3 to 10^6, and three volume fractions of the nanoparticles, namely, 0, 0.02, and 0.04.

Fig. 5 shows the streamlines and the isotherms in the annulus for the aspect ratio $AR = 1/4$, for different Rayleigh numbers and nanoparticles volume fractions. For this aspect ratio, the fluid is heated by the two sides of the inner square and expands as it moves upward. Subsequently, the fluid is cooled by the sides of the outer square and contracts as it moves downward. Hence, as Fig. 5-a shows, two counter-rotating eddies, a counterclockwise and a clockwise, are established in the left and the right halves of the annulus, respectively. These counter-rotating eddies are symmetric with respect to the vertical centreline of the squares (Fig. 5-a). The heat convection taking place from the central portion of the hot top surface of the inner square forms a streamline plume rising due to the flow of the fluid in the counter-rotating eddies in this region (Fig. 5-a).

For low Rayleigh numbers, i.e. a conduction-dominated heat transfer regime, the streamlines are, to some extent, evenly distributed within the two counter-rotating eddies. With increasing the Rayleigh number, the streamlines become more densely packed adjacent to the sides of the inner and the outer squares. Also, as Fig. 5-a indicates, the eyes of the counter-rotating eddies

Table 4
Average Nusselt number of the inner square for different uniform grids, $AR = 1/2$, $\varphi = 0.02$, and $Ra = 10^6$.

Number of nodes	21×21	41×41	61×61	81×81	101×101	121×121
Nu_{avg}	12.9555	13.02521	13.03912	13.04295	13.0430	13.0431

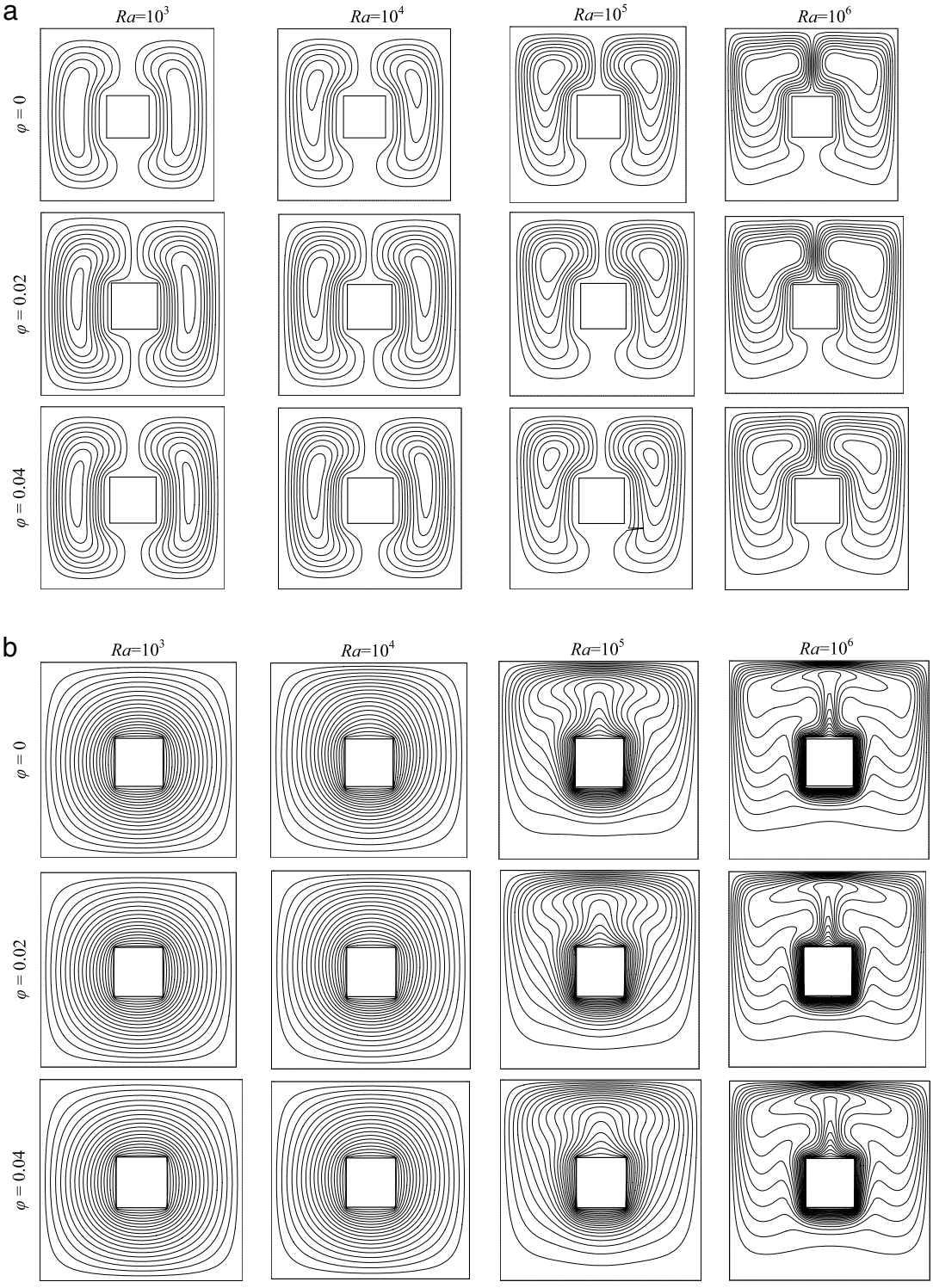

Fig. 5. Streamlines and isotherms in the space between concentric squares filled with TiO_2–water nanofluid for $AR = 1/4$: (a) streamlines, (b) isotherms.

move upwards as the Rayleigh number increases resulting in a more densely packed streamlines at the top portion of the annulus compared to its bottom. This further increase of the Rayleigh number also brings the two eyes of the counter-rotating eddies closes to each other so that the two counter eddies meet within the annulus top portion (Fig. 5-a).

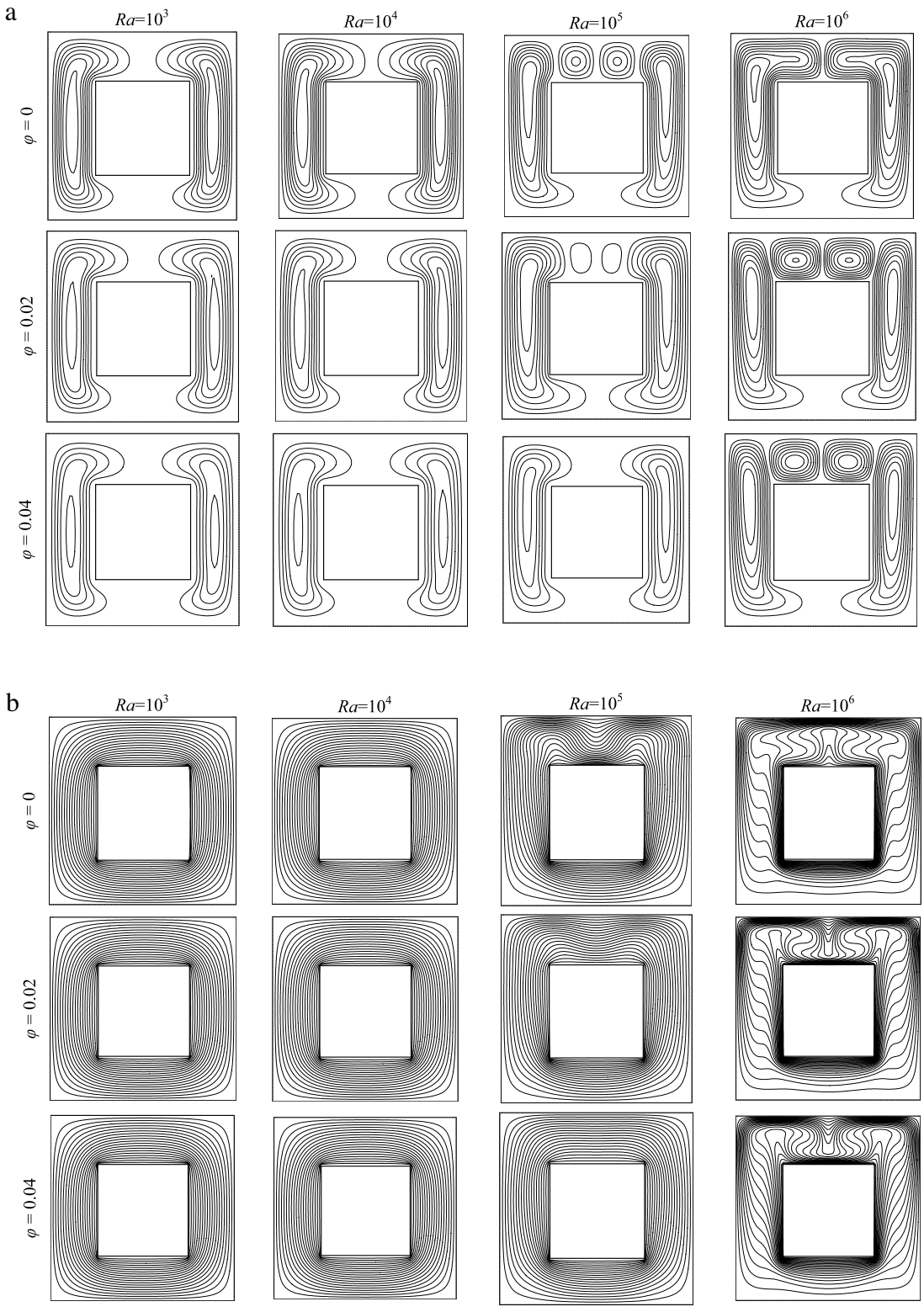

Fig. 6. Streamlines and isotherms in the space between concentric squares filled with TiO_2–water nanofluid for $AR = 1/2$: (a) streamlines, (b) isotherms.

As far as the isotherms are concerned, for $Ra = 10^3$ and 10^4, they are, in some ways, evenly distributed within the entire annulus demonstrating a conduction-dominated heat transfer regime (Fig. 5-b). For higher Rayleigh numbers, $Ra > 10^4$, when the natural convection effect become dominant, some distinct thermal boundary layers are formed around the inner square as well as along the sides of the outer square (Fig. 5-b). Furthermore, a thin thermal layer develops on the top surface of the inner square due to the two counter-rotating eddies and a strong plume rising above the inner square (Fig. 5-b). As it can be observed from Fig. 5-b, the core regions of the counter-rotating eddies are stratified for these cases. Moreover, the heat transfer in the bottom of the annulus is suppressed due to diminishing the conduction effect (Fig. 5-b). As far as the volume fraction of the nanoparticles, for high Rayleigh

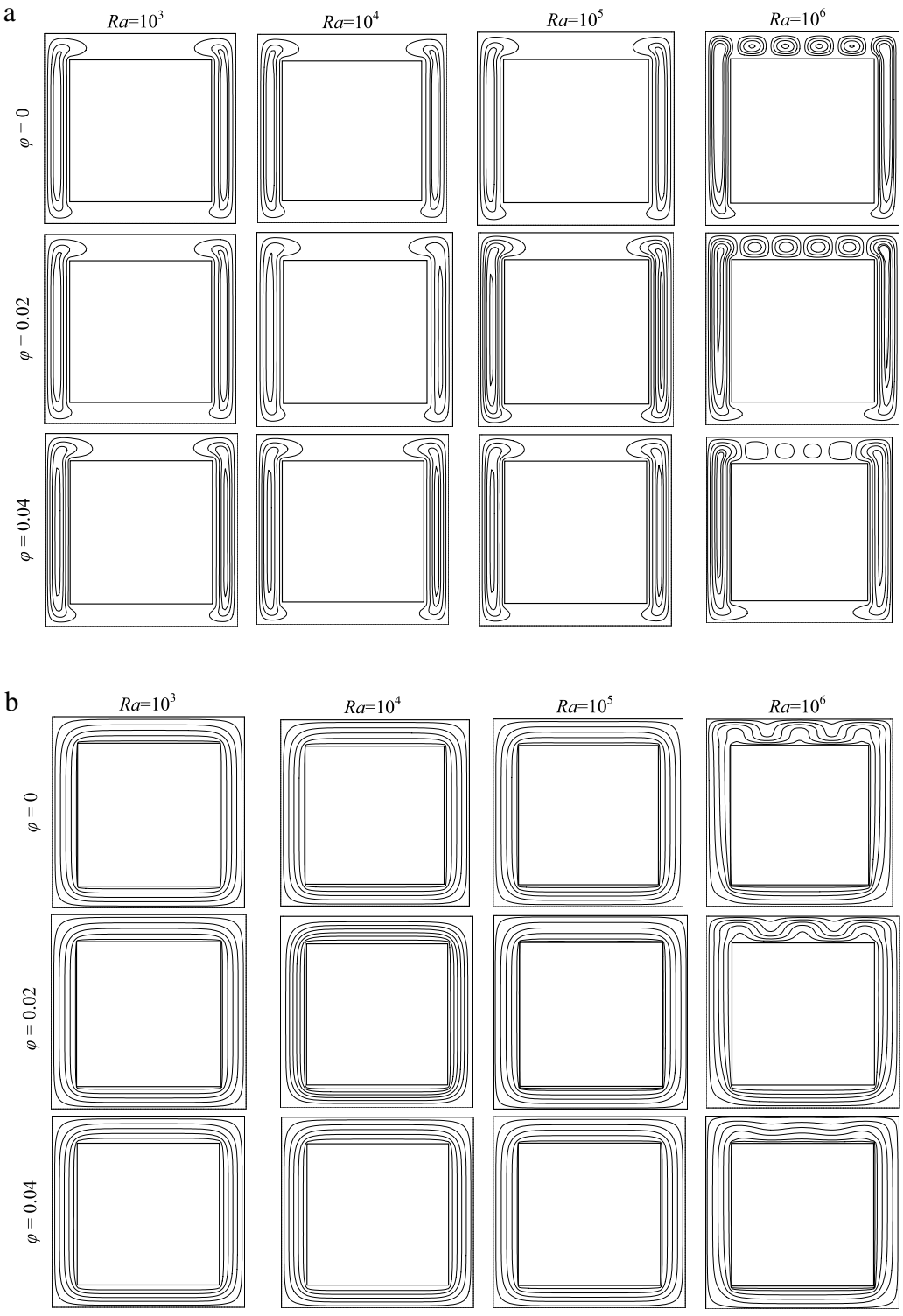

Fig. 7. Streamlines and isotherms in the space between concentric squares filled with TiO_2–water nanofluid for $AR = 3/4$: (a) streamlines, (b) isotherms.

numbers, the thermal boundary layers thicken, and the natural convection weakens due to increasing the nanofluid viscosity with increasing the volume fraction of the nanoparticles.

The streamlines and isotherms for $AR = 1/2$, different Rayleigh numbers, and nanoparticles volume fractions are presented in Fig. 6. For low Rayleigh numbers, $Ra \leq 10^4$, the streamlines and isotherms are quite similar to those shown in Fig. 5. However, as the gap between the squares gets narrower, the streamlines and isotherms become more densely packed inside the annulus. With increasing the Rayleigh number, two counter-rotating secondary eddies (similar to the Bénard cells) start to develop in the upper portion of the annulus above the inner square (Fig. 6-a). With further increase of the Rayleigh number, the secondary vortices start to die out, and the primary eddies move further inside the gap in the upper portion of the annulus. It must be mentioned here that, for a fluid layer between two sufficiently long horizontal plates heated from below, the condition for the onset of convection is expressed by the critical Rayleigh number, $Ra = 1708$, defined

based on the distance between the plates. For $Ra < 1708$, the fluid is quiescent and thermally stratified, while for $Ra > 1708$, cellular flow pattern develops in the fluid. For the cases shown in Fig. 6, the secondary eddies start to develop at a Rayleigh number defined based on the gap width approximately equal to 1200 which is lower than the critical Rayleigh number for long horizontal plates. The lower Rayleigh number for the onset of the cellular flow pattern is attributed to the fluid flow in the upper portion of the annulus due to the primary counter-rotating eddies.

As far as the volume fraction of the nanoparticles, for $Ra \leq 10^4$, the primary counter-rotating eddies weaken with increasing the volume fraction of the nanoparticles due to the viscosity increase of the nanofluid (Fig. 6-a). For $Ra = 10^5$, the secondary eddies start to die out with increasing the volume fraction of the nanoparticles and the resulting viscosity increase (Fig. 6-a). For higher Rayleigh numbers, e.g. $Ra = 10^6$, the primary eddies grow weaker in the upper portion of the annulus with increasing the viscosity of the nanofluid, and the secondary eddies begin to develop in this region. These eddies grow weaker with increasing the volume fraction of the nanoparticles (Fig. 6-a).

For $Ra \leq 10^4$, the isotherms in Fig. 6-b are evenly distributed in the annulus showing conduction-dominated heat transfer regimes. Contrary to the results in Fig. 5-b, for $Ra = 10^5$, the isotherms in Fig. 6-b still show a conduction-dominated heat transfer regime in the main portion of the annulus except in its top part where the secondary eddies are present. This is due to a reduction in the local Rayleigh number defined based on the gap width with increasing the aspect ratio AR. In the region above the top of the inner square, the isotherms get densely packed in the regions where a primary and its adjacent secondary eddies, or two secondary eddies move towards a wall. By moving away from the wall, the isotherms become separated (Fig. 6-b). For $Ra = 10^5$, the isotherms above the inner square become more evenly distributed with increasing the volume fraction of the nanoparticles and the resulting suppression of the secondary eddies (Fig. 6-b). For $Ra = 10^6$, distinct thermal boundary layers are formed around the inner square, and along the sides and the top of the outer square. The rest of the annulus is nearly thermally stratified (Fig. 6-b).

The streamlines and the isotherms in the annulus for the aspect ratio $AR = 3/4$, and different Rayleigh numbers and nanoparticles volume fractions are shown in Fig. 7. As it can be observed from this figure, with decreasing the width of the gap between the concentric squares, and the resulting decrease of the local Rayleigh number, the conduction-dominated heat transfer regime persists within the entire gap for up to $Ra = 10^5$ (Fig. 7-a, b). This is clearly observed from the evenly distributed isotherms of Fig. 7-b for $Ra \leq 10^5$. The primary counter-rotating eddies are quite weak for $Ra \leq 10^5$. For $Ra = 10^6$, the local Rayleigh number defined based on the gap width is sufficiently high so that the Bénard cells, four counter-rotating two-dimensional rolls, develop in the relatively long and narrow gap in the top portion of the annulus (Fig. 7-a). These secondary eddies begin to die out with increasing the volume fraction of the nanoparticles and the viscosity of the nanofluid. As it can be observed from Fig. 7-b, for $Ra = 10^6$, the isotherms above the inner square become evenly distributed with increasing the nanoparticles volume fraction.

Fig. 8 shows the variation of the average Nusselt number of the outer square with respect to the Rayleigh number for various volume fractions of the nanoparticles, and the aspect ratios of 1/4, 1/2, and 3/4. As it can be seen from this figure, for $AR = 1/4$ and 1/2, the average Nusselt number of the cold square generally increases with increasing the Rayleigh number, i.e. as the heat transfer regime becomes convection-dominated. For $AR = 1/4$, the average Nusselt number remains nearly constant for $Ra \leq 10^4$, while for $AR = 1/2$, it remains practically constant if the Rayleigh number is less than or equal to 10^5. In both of these

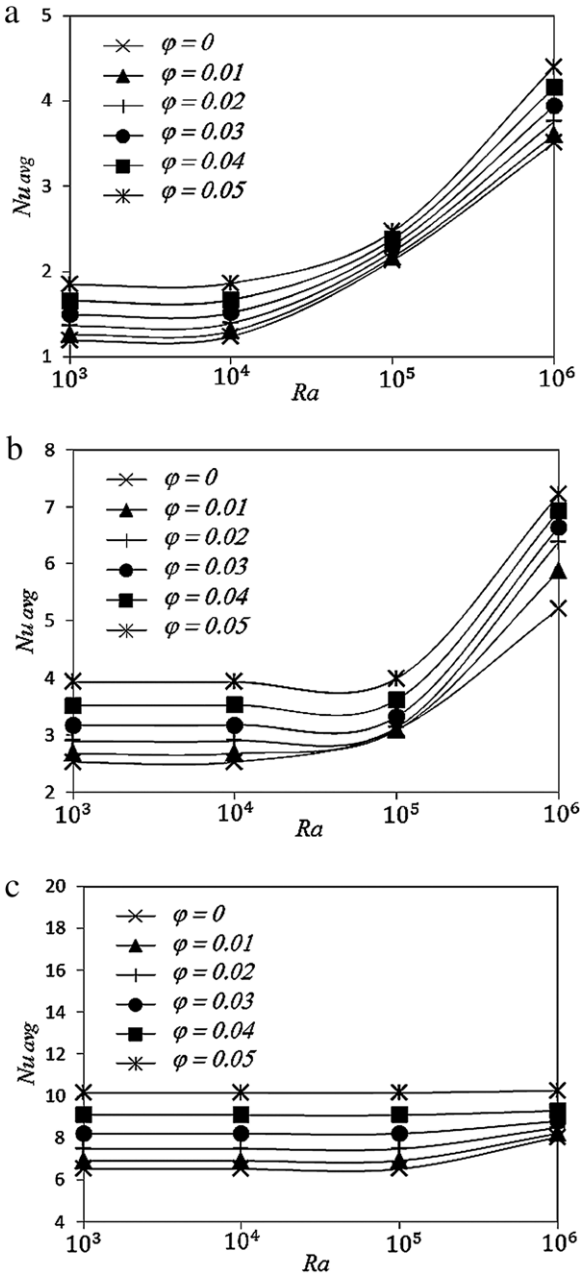

Fig. 8. Average Nusselt number variation for the outer square for (a) $AR = 1/4$, (b) $AR = 1/2$, (c) $AR = 3/4$.

cases, the heat transfer regime is conduction-dominated (Fig. 8-a, b). Moreover, the average Nusselt number of the cold square, in general, increases with increasing the volume fractions of the nanoparticles. For $AR = 3/4$, the Rayleigh number has negligible effects on the average Nusselt number up to $Ra = 10^5$. This is due to the fact that for $AR = 3/4$ the width of the gap between the squares is quite small, and the heat transfer occurs basically through conduction.

5. Conclusions

Heat transfer and fluid flow analysis of the TiO_2–water nanofluid flow within two-square duct annuli are conducted to determine the implication of a number of the natural convection heat transfer characteristics.

The finite volume method together with the SIMPLER algorithm is implemented to solve the governing equations written in terms of the primitive variables. The numerical procedure is verified via

two different simulations, a buoyancy-driven fluid flow and heat transfer in a differentially-heated square cavity filled with air, and a buoyancy-driven heat transfer in a partially-heated square cavity with the Cu–water nanofluid.

A parametric study involving the effects of the Rayleigh number, annulus aspect ratio, and the TiO_2 volume fraction on the annuli fluid flow and heat transfer are conducted. The results, in general, show that high Rayleigh number is eminently an effective parameter causing the formation of the multiple vortices of the Rayleigh–Bénard convective type within the top portion of the annuli. Larger widths of the annulus, however, seem to strengthen these developed vortices.

Although the general trend of the average Nusselt number profiles versus the Rayleigh number for both the traditional fluid and the TiO_2–water nanofluid follow the same pattern, the distribution, however, clearly distinguish the natural convection heat transfer much improvements in the presence of the nanoparticles.

References

[1] L. Godson, B. Raja, D.M. Lal, S. Wongwises, Enhancement of heat transfer using nanofluids—An overview, Renew. Sust. Energ. Rev. 14 (2010) 629–641.

[2] J. Buongiorno, Convective transport in nanofluids, J. Heat Transf. 128 (2006) 240–250.

[3] K. Khanafer, K. Vafai, M. Lightstone, Buoyancy-driven heat transfer enhancement in a two-dimensional enclosure utilizing nanofluid, Int. J. Heat Mass Transf. 46 (2003) 3639–3653.

[4] R. Jou, Sh. Tzeng, Numerical research of nature convective heat transfer enhancement filled with nanofluids in rectangular enclosures, Int. Comm. Heat Mass Transf. 33 (2006) 727–736.

[5] E. Abu-Nada, Z. Masoud, A. Hijazi, Natural convection heat transfer enhancement in horizontal concentric annuli using nanofluids, Int. Comm. Heat Mass Transf. 35 (2008) 657–665.

[6] A.K. Santra, S. Sen, N. Chakraborty, Study of heat transfer augmentation in a differentially heated square cavity using copper–water nanofluid, Int. J. Therm. Sci. 47 (2008) 1113–1122.

[7] H.F. Oztop, E. Abu-Nada, Numerical study of natural convection in partially heated rectangular enclosures filled with nanofluids, Int. J. Heat Fluid Flow 29 (2008) 1326–1336.

[8] E. Abu-nada, H. Oztop, Effect of inclination angle on natural convection in enclosures filled with Cu–water nanofluid, Int. J. Heat Fluid Flow 30 (2009) 669–678.

[9] E.B. Ögüt, Natural convection of water-based nanofluids in an inclined enclosure with a heat source, Int. J. Therm. Sci. 48 (2009) 2063–2073.

[10] S.M. Aminossadati, B. Ghasemi, Natural convection cooling of a localized heat source at the bottom of a nanofluid-filled enclosure, Eur. J. Mech. B/Fluids 28 (2009) 630–640.

[11] B. Ghasemi, S.M. Aminossadati, Periodic natural convection in a nanofluid-filled enclosure with oscillating heat flux, Int. J. Therm. Sci. 49 (2010) 1–9.

[12] S. Gumguma, M. Tezer-Sezgin, DRBEM solution of natural convection flow of nanofluids with a heat source, Eng. Anal. Bound. Elem. 34 (2010) 727–737.

[13] R. Ni, S.Q. Zhou, K.Q. Xia, An experimental investigation of turbulent thermal convection in water-based alumina nanofluid, Phys. Fluids 23 (2011) 022005-1–022005-12.

[14] M. Jahanshahi, S.F. Hosseinizadeh, M. Alipanah, A. Dehghani, G.R. Vakilinejad, Numerical simulation of free convection based on experimental measured conductivity in a square cavity using Water/SiO_2 nanofluid, Int. Comm. Heat Mass Transf. 37 (2010) 687–694.

[15] H.F. Oztop, E. Abu-Nada, Y. Varol, K. Al-Salem, Computational analysis of non-isothermal temperature distribution on natural convection in nanofluid filled enclosures, Superlattic. Microstruct. 49 (2011) 453–467.

[16] G.A. Sheikhzadeh, A. Arefmanesh, M.H. Kheirkhah, R. Abdollahi, Natural convection of Cu–water nanofluid in a cavity with partially active side walls, Europ. J. Mech. B/Fluids 30 (2011) 166–176.

[17] G.A. Sheikhzadeh, A. Arefmanesh, M. Mahmoodi, Numerical study of natural convection in a differentially-heated rectangular cavity filled with TiO_2–water nanofluid, J. Nano Res. 13 (2011) 75–80.

[18] Z. Alloui, P. Vasseur, M. Reggio, Natural convection of nanofluids in a shallow cavity heated from below, Int. J. Therm. Sci. 50 (2011) 385–393.

[19] B. Ghasemi, S.M. Aminossadati, Brownian motion of nanoparticles in a triangular enclosure with natural convection, Int. J. Therm. Sci. 49 (2010) 931–940.

[20] A. Bejan, Convection Heat Transfer, John Wiley & Sons, Inc., Hoboken, New Jersey, USA, 2004.

[21] Y. He, Y. Men, Y. Zhao, H. Lu, Y. Ding, Numerical investigation into the convective heat transfer of TiO_2 nanofluids flowing through a straight tube under the laminar flow conditions, Appl. Therm. Eng. 29 (2009) 1965–1972.

[22] S.V. Patankar, Numerical Heat Transfer and Fluid Flow, Hemisphere Publishing Corporation, Taylor and Francis Group, New York, 1980.

[23] G. Barakos, E. Mitsoulis, Natural convection flow in a square cavity revisited: laminar and turbulent models with wall fraction, Int. J. Numer. Meth. Fluid. 18 (1994) 695–719.

[24] G.V. Davis, Natural convection of air in a square cavity, a benchmark numerical solution, Int. J. Numer. Meth. Fluid. 3 (1983) 249–264.

[25] T. Faseqi, J.M. Hyun, K. Kawahara, B. Farouk, A Numerical study of tree–dimensional natural convection in a differentially heated cubical enclosure, Int. J. Heat Mass Transf. 34 (1991) 1543–1557.

[26] N.C. Markatos, K.A. Pericleous, Laminar and turbulent natural convection an enclosed cavity, Int. J. Heat Mass Transf. 27 (1984) 772–775.